Clay Minerals (2006) **41**, 791–809

Thermal models and clay diagenesis in the Tertiary-Cretaceous sediments of the Alava block (Basque-Cantabrian basin, Spain)

J. AROSTEGUI[1,*], F. J. SANGÜESA[1], F. NIETO[2] AND J. A. URIARTE[3]

[1] *Departamento de Mineralogía y Petrología, Facultad de Ciencia y Tecnología, Universidad del País Vasco/EHU, Apdo. 644, 48080, Spain,* [2] *Departamento de Mineralogía y Petrología, IACT, Universidad de Granada-CSIC, 18002 Granada, Spain, and* [3] *Departamento de Geodinámica, Facultad de Ciencia y Tecnología, Universidad del País Vasco/EHU, Apdo. 644, 48080, Spain*

(*Received 1 March 2006; revised 24 July 2006*)

ABSTRACT: Diagenesis in the Cretaceous and Tertiary sediments of the Alava Block (Basque-Cantabrian basin) has been studied using the clay mineralogy (X-ray diffraction) of cuttings from three representative wells of a N–S cross-section. More than 5500 m of various lithologies (marls, mudstones and sandstones) have been drilled in the northern part of the domain, and 2100 m in the southern zone. The illitization of smectite and the disappearance of kaolinite, due to diagenesis, are the most characteristic features in the northern well. Evolution of smectite to illite has been differentiated into four zones, from top to bottom of the series, each showing specific I-S interstratified clay assemblages. The disappearance of smectite and the distribution of kaolinite in the other two wells are explained based on source-area considerations. Burial and thermal history have been reconstructed, revealing a northward increase in thermal flow until the Oligocene (Alpine orogeny paroxysm). In the northern well, the thermal model suggests temperatures of 160 and 270ºC for the disappearance of smectite (R0) and illite-smectite (I-S) mixed-layer R1 clay minerals, respectively. The disappearance of kaolinite is related to a temperature of 230ºC, a temperature never attained in the other two wells. Retardation of these processes, in relation to temperature values in the literature, is a consequence of the poor reactivity of marly lithologies, due to the low availability of cations. In this regard, the scarcity of reactants (K-bearing phases) and the absence of pathways (low permeability) for their access and circulation imply that illitization could have taken place in a closed system, by diffusion, on a very small scale, i.e. that of the original smectite grains.

KEYWORDS: Basque-Cantabrian Basin, diagenesis, wells, marls, thermal modelling, illite-smectite, temperature, illitization, retardation.

Thermal modelling of sedimentary basins has attracted increasing attention in recent decades due to its application as a tool in hydrocarbon exploration, i.e. oil or gas generation and possible paths of hydrocarbon migration (Tissot *et al.*, 1987; Waples *et al.*, 1992; Yahi *et al.*, 2001). Temperature values obtained from these models have frequently been related to clay mineral distribution in diagenetic series (Pearson & Small, 1988; Glansman *et al.*, 1989; Velde & Lanson, 1993; Schegg & Leu, 1996) and to organic maturity indicators, mainly vitrinite reflectance (Gier, 2000). Although a direct correspondence between time/temperature and organic maturity exists in many sedimentary basins, correspondence with clay mineral composition is not as common, as it depends on several additional factors (Scotchman, 1987; Merriman, 2005). Most research dealing with

* E-mail: javier.arostegi@ehu.es
DOI: 10.1180/0009855064140219

relationships between clay mineralogy and burial temperature has focused on sandstones and shales, with the clay diagenesis of carbonate sediments receiving very little attention.

We have studied the Alava Block (included in the Basque-Cantabrian Basin), which presents laterally correlated sandstone, shale and carbonate stratigraphic series, buried at different depths. This stratigraphic scenario has allowed us to study the clay mineral evolution with increasing temperature of burial, without the influence of lithological variables. In a previous work, Sangüesa *et al.* (2000) analysed the origin of clay minerals in the Lower Cretaceous of the Alava Block. Based on scanning electron microscopy observations, they deduced the presence of authigenic clay minerals in sandstones and proposed temperature ranges for their formation.

In this paper we present thermal models of the complete depositional history of three hydrocarbon wells. These wells are representative of the space-time evolution of the sedimentary environment of the Alava Block, and offer some data for the calibration of the models based on present-day temperatures from one of the wells, and vitrinite reflectance values for all three. Clay mineral distribution, particularly indicators of the diagenetic history such as smectite illitization steps and kaolinite disappearance, are evaluated in the most realistic thermal and burial history stages of the studied wells, in accordance with the complete geological history of the basin and available calibration data. The aim of this study is to understand the relative influence of various factors on mineral changes in different wells. Variables examined include the composition of rocks in the source area, the lithology of the sedimentary rock, and depth/time and temperature of burial.

GEOLOGICAL SETTING

The study area is located in the Alava Block domain (Rat, 1988) of the Basque-Cantabrian Basin (Fig. 1). Its geological history is related to the opening and closing of the Gulf of Vizcaya, which is closely connected with the geodynamic evolution of the North Atlantic. In this area, Cretaceous and Tertiary sedimentation was controlled by deep

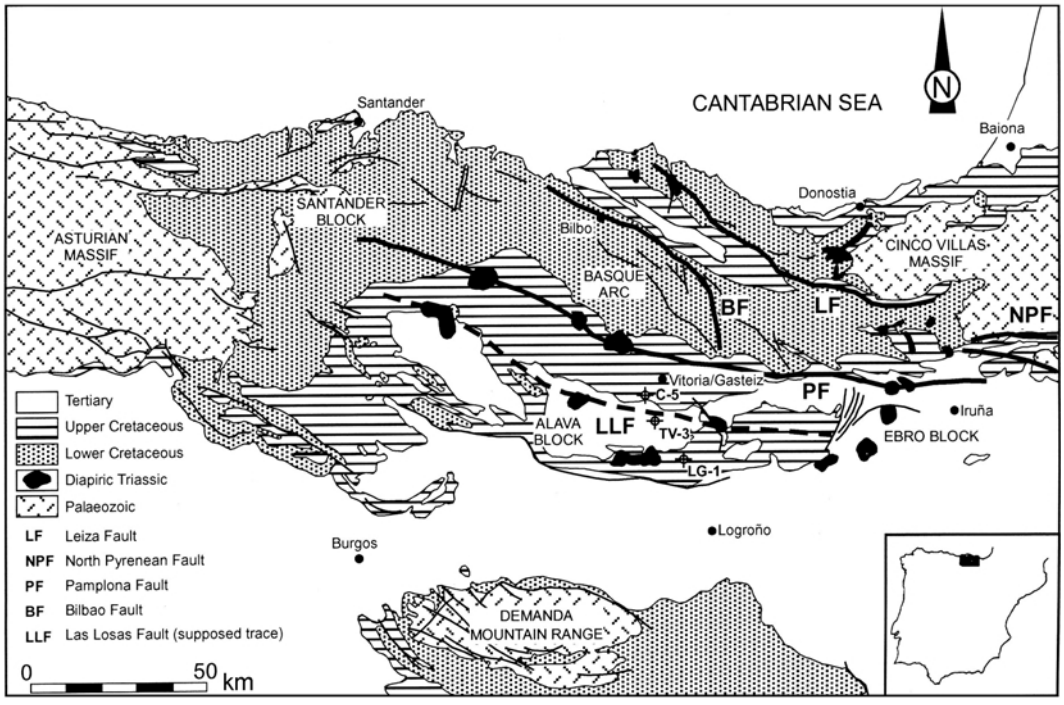

FIG. 1. Geological setting of the Alava Block, showing the locations of the three wells. In this and following figures, C-5: Castillo-5, TV-3: Treviño-3 and LG-1: Lagran-1.

(NW–SE) faulting, which determined the shoreline during the depositional history of this domain. In this paper, we present data on three deep wells: Lagran-1, Treviño-3 and Castillo-5. These wells are representative of the lateral and vertical evolution of the sedimentary environment in Cretaceous and Tertiary times, and are located along a line where distality increases northwards.

The main stratigraphic feature of the Alava Block (Fig. 2) is the presence of thick Cretaceous and Tertiary series, ranging from 2100 m at the southern end (Lagran-1) to 5500 m in the northern end.

Outcrops of Lower Cretaceous materials (Sangüesa *et al.*, 2000), very scarce in the region, consist of detrital sediments (fluvial-deltaic sandstones and shales) with intercalated carbonate (Urgonian facies) episodes. Upper Cretaceous materials are mainly carbonates (limestones and marls) deposited on a marine platform, progressively deeper northwards. Sedimentation during the Upper Cretaceous shows great cyclicity due to eustatic events, so that four lithological intervals (UC1 to UC4 in Fig. 2), corresponding to four sedimentary macrosequences (Gräfe & Wiedmann, 1993), are differentiated in the wells. Their limits coincide with shallowing events reflected throughout the entire basin (Amiot *et al.*, 1983).

Tertiary sediments are only present in the central sector of the Alava Block, seen in well Treviño-3. They consist of three different sedimentary cycles, only one of which (Oligocene-Miocene) is conserved in this well. It is made up of a syn/post-orogenic continental series comprising dolomites and sandy limestones in lacustrine and alluvial facies.

SAMPLES AND ANALYTICAL METHODS

Mineralogy

120 samples of cuttings from the three wells were analysed. These samples, mainly shales and marls, were collected at ~100 m intervals depending on the homogeneity of each lithological

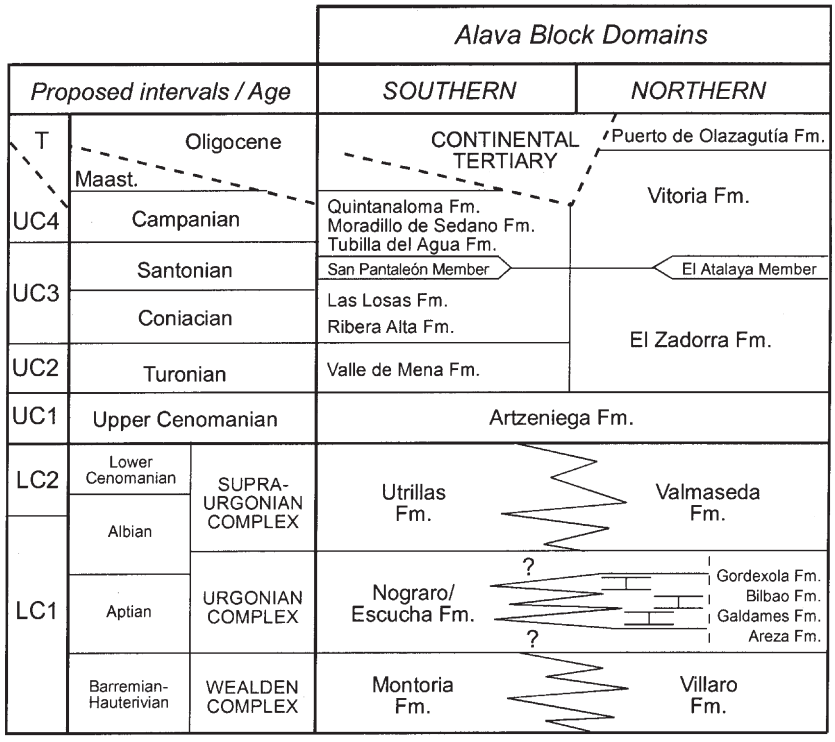

FIG. 2. Schematic stratigraphy of the Alava Block and its relationship with the proposed intervals. Modified from García-Mondejar (1982) and Amiot (1982). LC: Lower Cretaceous, UC: Upper Cretaceous, T: Tertiary.

interval. They were washed with de-ionized water and gently crushed with a laboratory jaw-crusher.

Randomly orientated powders of the bulk sample were used to characterize the whole-rock mineralogy by X-ray diffraction (XRD). The <2 μm fraction was separated by centrifugation, and then smeared onto glass slides. In some cases, it was first necessary to remove carbonates. A solution of 0.2 N HCl was therefore added to a suspension of crushed rock and agitated continuously for 10 min.

Clay minerals in this fraction were identified according to the position of the (00l) series of basal reflections on XRD patterns of air-dried, ethylene-glycolated, and heated (at 550ºC for 2 h) specimens (Moore & Reynolds, 1997). The presence of kaolinite was also checked on XRD patterns after solvation with dimethyl sulphoxide. Illite-smectite (I-S) mixed-layer clay minerals, smectite-rich R0 (<50%I) and illite-rich R1 (60–80%I) and R3 (>80%I), were also identified (Środoń & Eberl, 1984; Moore & Reynolds, 1989). Routine semi-quantitative estimates were made from peak areas on XRD patterns both for bulk-rock mineralogy and for clay mineralogy in the separated fine fraction.

Experimental XRD patterns of almost all samples from well Castillo-5 (in contrast with the other two wells) show a very broad, diffuse band associated with the 001 illite peak (10 Å) in the low-angle region, which is only partially resolved after glycol solvation. To further resolve this band, the DECOMPXR decomposition software (Lanson & Besson, 1992; Lanson & Velde, 1992) has been used in the 5–11º2θ angular interval of XRD patterns of air-dried and glycol-solvated samples. The presence of chlorite, detrital mica and quartz in all the samples, together with small amounts of mixed-layer I-S, have prevented decomposition in other regions of the profile (Lanson & Velde, 1992). It has been necessary to use a different total number of elementary contributions in each sample to obtain an acceptable fitting (reliability factor >99.5%). Nevertheless, we have observed good consistency in the decomposition of both types of patterns (air-dried and ethylene-glycolated) for the 2θ region. Likewise, the relative proportions of each subpopulation have been estimated from different intensity ratios (integrated area). In the case of illite-rich (R1 and R3) I-S, the relationships between position (*d*, Å) and full-width (FWHM, º2θ) parameters for each elementary peak have been obtained from Lanson's (1997) diagram. The NEWMOD program has allowed us to simulate illite and different I-S types (R0, R1 and R3), considering various % illite in I-S and different crystallite sizes and distributions (*N*).

Thermal modelling

Burial and thermal histories have been modelled for the three wells with the PetroMod 1D Basin Modeling software from IES GmbH, Jülich (Germany). This program carries out a numerical simulation that requires:

(1) Definition of deposition, non-deposition, and erosion events affecting the stratigraphic log of the well, using several parameters from each lithological interval such as thickness, lithology and age.

(2) Fixing of the limiting conditions: palaeowater depth (PWD), sea-water interface temperature (SWI) for each depositional event, and heat-flow (HF) history. The PWD values have been deduced from the facies type for each event. Moreover, different HF trends have been modelled, keeping in mind the geodynamic evolution of the basin in the context of plate tectonics.

(3) Thermo-physical (thermal conductivity and heat capacity) and mechanical (compressibility, porosity, permeability, etc.) parameters are integrated in the model by the software from defined lithotypes and limiting conditions, mainly the HF trend and burial history of the well.

(4) The validity of the assumed thermal history has been verified by two calibration parameters: the corrected bottom-hole temperature (BHT) data of Arostegui & Uriarte (1991) and the vitrinite reflectance data from different lithostratigraphic intervals, previously reported by Sangüesa *et al.* (2000). By means of successive iterations, thermal flow was modified until good agreement was obtained between calculated and measured calibration data.

RESULTS

Whole-rock mineralogy

Taking into account the lithology of these wells, two thick interval sequences (Fig. 3) can be defined: the first (Lower Cretaceous) is detrital, mainly composed of sandstones and shales, with intercalated Urgonian carbonatic episodes; the second, upper, interval sequence is rich in carbonate rocks (Upper Cretaceous and Tertiary). The

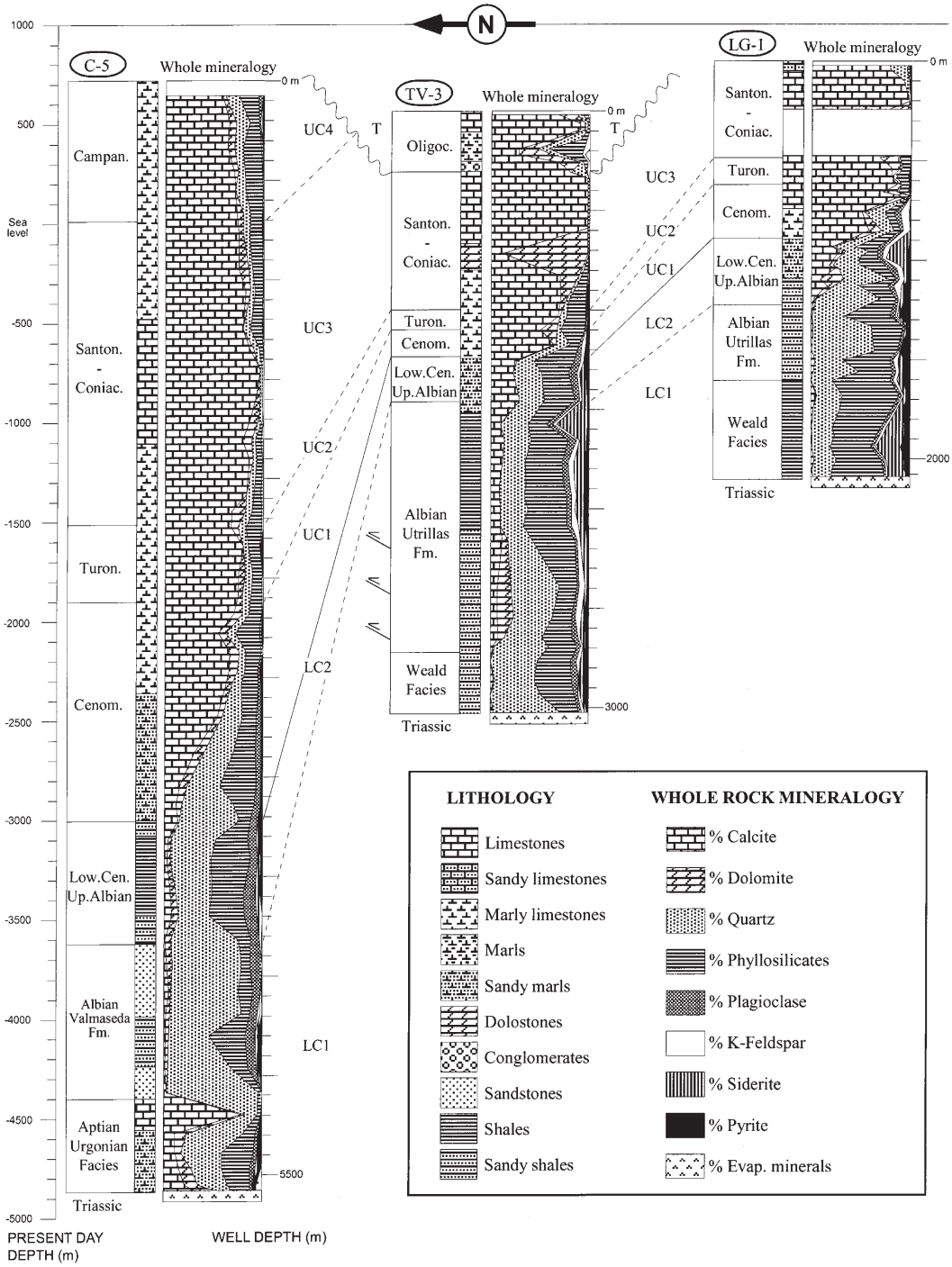

FIG. 3. Distribution of whole-rock mineralogy in the three wells from the Alava Block, showing its correlation with the lithostratigraphic units. (LC: Lower Cretaceous, UC: Upper Cretaceous, T: Tertiary). Simplified stratigraphy and present-day depth are also shown.

transition between these major lithological interval sequences is more or less gradual.

The mineral composition of the Lower Cretaceous sediments (intervals LC1 and LC2) is clearly detrital in origin, with 50% quartz, 23% phyllosilicates and 8% feldspars as principal components. Siderite (4%) is also present. The Upper Cretaceous rocks show a progressive increase in carbonate, from ~50% calcite in UC1 to 95% calcite in UC3, where the calcite begins a decrease that reaches 60–70% in UC4 (well Castillo-5). In all cases, the remaining mineral composition consists of quartz and phyllosilicates. The mineral distribution of Tertiary sediments (well Treviño-3) is very heterogeneous, with carbonates (60% calcite and 5–34% dolomite) being more abundant than detrital minerals (10% quartz, 2–36% phyllosilicates, and <5% K-feldspar).

Clay mineralogy (<2 μm fraction)

The distribution of clay minerals in the <2 μm fraction is shown in Fig. 4. Mineralogical data for the Lower Cretaceous are from Sangüesa *et al.* (2000). Mica is the most abundant clay mineral in all samples from the three wells. Illite-smectite (I-S) mixed-layer minerals correspond to the randomly interstratified R0 type (smectite-like) with a small proportion of illite layers, and illite-rich ordered R=1 and R=3 types. Kaolinite and chlorite are also present, with a scattered distribution.

Distribution of illite and mixed-layer I-S clays

Mica is present in all samples, is the major phase in most of them, and shows a slight increase with depth.

The upper sections of the three wells are characterized by a significant proportion of R0 randomly mixed-layered I-S that disappears in the lower sections (Fig. 4). In wells Lagran-1 and Treviño-3, R0 is present in Tertiary–Lower Cretaceous sediments; toward the bottom (interval LC1), R0 is absent and illite is clearly predominant, with only very small amounts of R1 I-S in a few samples.

In Castillo-5, R0 mixed-layer clays are present down to the Santonian-Coniacian sediments (UC3). Deeper, these materials are completely replaced by illite-rich R1 and R3 type I-S, although in different relative proportions. The decomposition results of the XRD patterns in this well allow them to be grouped into four different types on the basis of distinctive mixed-layer I-S and mica distributions.

These types correspond with lithostratigraphic intervals from increasing depth, exemplified by several samples from different well depths (Fig. 5 and Table 1).

In the shallowest samples (335 and 775 m), the mixed-layer assemblage is made up of R0 smectite-rich I-S (between 15 and 25% I), illite-rich I-S (75% I on average) with R1 ordering, and illite-rich I-S (90–100% I) with R3 ordering. In both samples, decomposition of the 10 Å reflection requires only one elementary peak, the parameters of which indicate 98–100% I and a coherent scattering domain size (CSDS) of 22–39 layers, typical of a well crystallized illite (WCI).

Below 1640 m (1915 m sample in Fig. 5), the most remarkable feature is the absence of R0. R1 is the major illite-rich I-S (R1-R3 ratio >1). The percentage of illite in both I-S does not vary in the shallower samples; the CSDS for R3 ordered I-S is similar (Table 1). The reflection at 10 Å is again explained by a WCI, the parameters of which indicate 100% I and a CSDS of 22–39 layers.

In the 3735 m sample, R1 and R3 I-S mixed-layer clays are also present, but R3 is more abundant (R1/R3 ratio <1). In this sample, the illite reflection at 10 Å can be decomposed into two peaks, corresponding to a poorly crystallized illite (PCI) with 90–100% illite (6–14 layers), and to a WCI with 100% illite and a CSDS of 22–39 layers.

In this well, below 4400 m, I-S mixed-layer clays are entirely absent and only trace amounts of R3 can be detected in addition to the predominant illite. The decomposition of the profile corresponding to the sample from 5458 m shows R3 and illite, nearly the only phase present. Illite is represented by PCI and WCI subpopulations, with similar characteristics to the previous sample (Table 1).

Kaolinite and chlorite distribution

Kaolinite shows great differences in vertical distribution for the three wells. In Lagran-1 and Treviño-3, kaolinite is present along the entire sequence, with no significant lateral differences. Kaolinite increases with depth from the Upper Cretaceous towards the Lower Cretaceous, but has not been detected in the Lower Cretaceous of Castillo-5 despite the similarity in lithologies, shales and sandy shales.

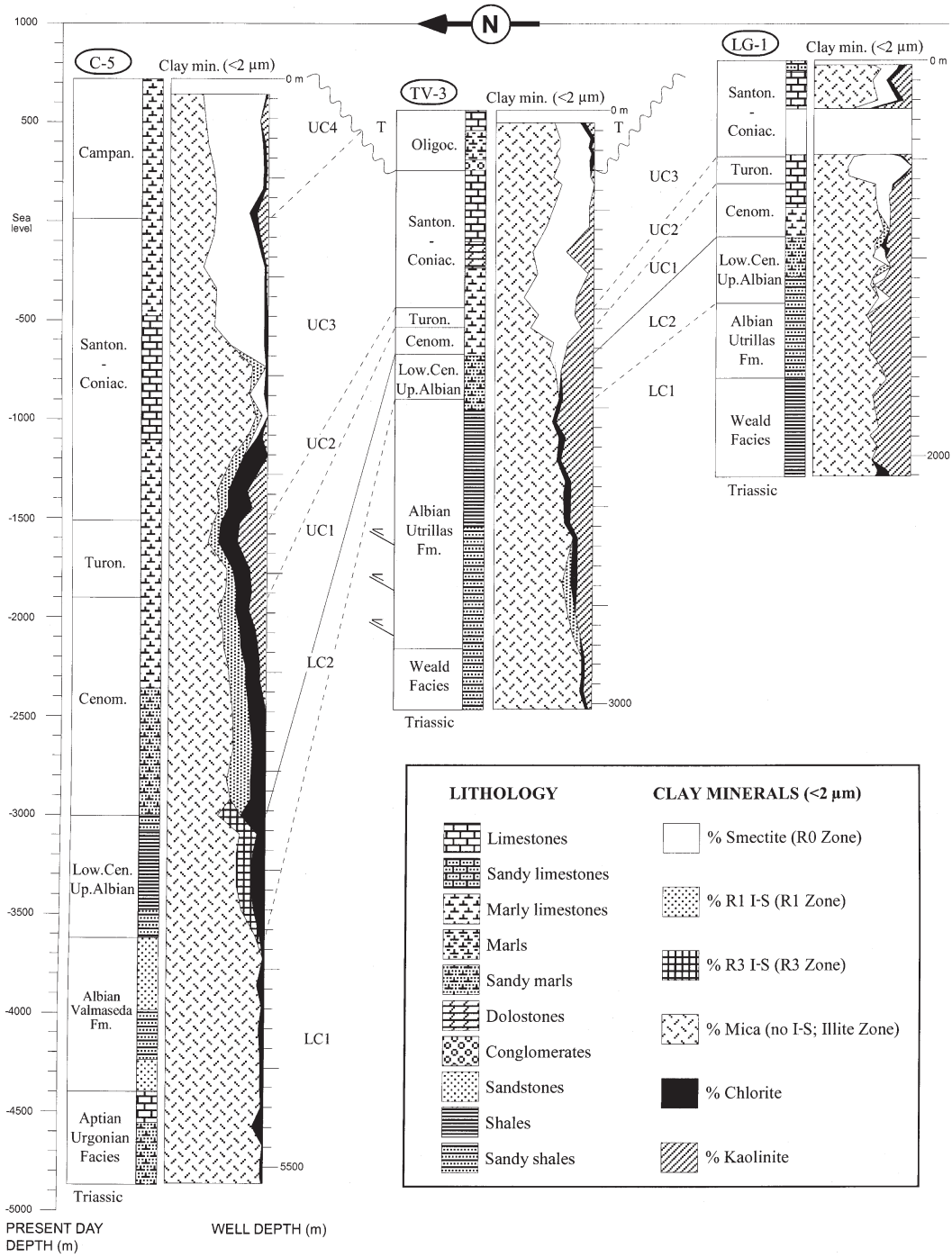

FIG. 4. Distribution of clay minerals (<2 µm fraction) in the three wells (see also Fig. 5).

Chlorite distribution does not fall into any specific pattern. It is very scarce or even absent in Treviño-3 and Lagran-1. On the other hand, in Castillo-5 chlorite is ubiquitous, appearing in significant

TABLE 1. Main features of the different sub-populations of I-S and illite identified by means of XRD profile decomposition (DECOMPXR; Lanson and Besson, 1992) of samples from the well Castillo-5.

Sample	Param.	R0	R1	R3	PCI	WCI	Ratio	
	d (Å) (1)	14.59	12.17	10.41		10.01	0.3	R0/R1+R3
	%I (2)	–	–	90–100		(98–100)	3.3	R1/R3
335 m	%I (3)	17	70–80	–	absent	–	4	I-S/illite
	FWHM	1.15º	1.78º	0.90º		0.33º		
	CSDS (4)	(2–9)	–	6–14 (6–14)		36–39 (22–39)		
	d (Å) (1)	14.84	12.22	10.60		10.07	0.5	R0/R1+R3
	%I (2)	–	–	90–100		(98–100)	4.9	R1/R3
795 m	%I (3)	28	60	–	absent	–	5.7	I-S/illite
	FWHM	1.29º	1.62º	0.87º		0.40º		
	CSDS (4)	(2–9)	–	2–9 (6–19)		22–39 (16–25)		
	d (Å) (1)		11.46	10.50		10.02	0	R0/R1+R3
	%I (2)		–	90–100		(98–100)	2.4	R1/R3
1915 m	%I (3)	absent	70–80	–	absent	–	4.2	I-S/illite
	FWHM		1.46º	0.93º		0.33º		
	CSDS (4)		–	6–14 (6–19)		36–39 (22–39)		
	d (Å) (1)		12.19	10.67	10.23	9.99	0	R0/R1+R3
	%I (2)		–	90	90–100 (98–100)	(99–100)	0.5	R1/R3
3735 m	%I (3)	absent	70–80	–	–	–	1.6	I-S/illite
	FWHM		1.3º	1.13º	0.63º	0.30º		
	CSDS (4)		(2–9)	6–14 (6–14)	6–14 (6–14)	36–39 (22–39)		
	d (Å) (1)			10.78	10.16	9.97	0	R0/R1+R3
	%I (2)			90–100	100 (100)	(99–100)	0	R1/R3
5458 m	%I (3)	absent	absent	–	–	–	0.1	I-S/illite
	FWHM			1.03º	0.50º	0.24º		
	CSDS (4)			2–9 (6–14)	11–19 (11–19)	36–39 (36–39)		

(1) air-dried position; (2) according to Lanson (1997); (3) according to Moore and Reynolds (1997); (4) according to Lanson (1997) and from Newmod program (in parenthesis). PCI – poorly crystallized illite; WCI – well crystallized illite

amounts in the 1000–3600 m interval, both in detrital materials (shales and sandy shales,) and marls.

BURIAL AND THERMAL MODELLING

Burial history

The creation of a sedimentary basin evolutionary model requires burial and thermal quantification of the basin over time. This is difficult for the Alava Block, as is the geological history of the basin itself. The burial history we have constructed required a number of suppositions, so the resulting models (Fig. 6) must be considered simply as an approximation to the real history, although they are founded on currently available data.

In the study area, two major depositional phases have been distinguished. The first extends until the Eocene, and is the most modern stratigraphic record in this region of Ypresian (55–49 Ma) age. This phase is characterized by continuous sedimentation in the entire region until the Upper Santonian, according to the tectonic seating of strongly subsident blocks, controlled by deep NW–SE faults. From this age, a new onset of subsidence (Amiot *et al.*, 1983) took place. While the deposition of transgressive facies (Vitoria Fm.) continued in the northern sector (Castillo-5), the deposition of regressive facies had begun in the southern one (Lagran-1) (Fig. 2). Due to differential subsidence, the thickness of accumulated sediment was much greater in the northern sector.

During the Alpine orogeny paroxysm (Upper Eocene, 34 Ma), erosion took place in the northern

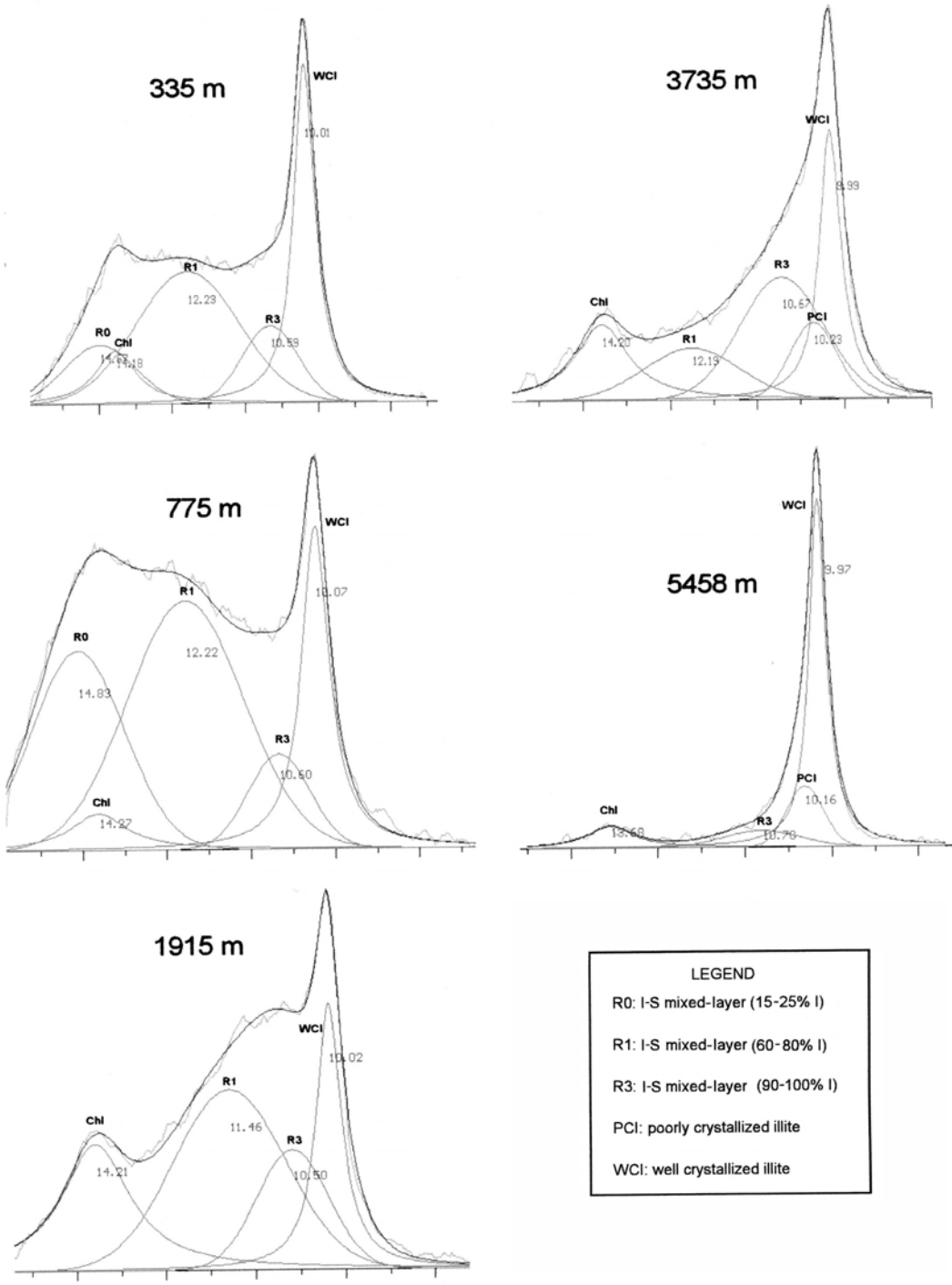

FIG. 5. Decomposition of XRD patterns for the well Castillo-5.

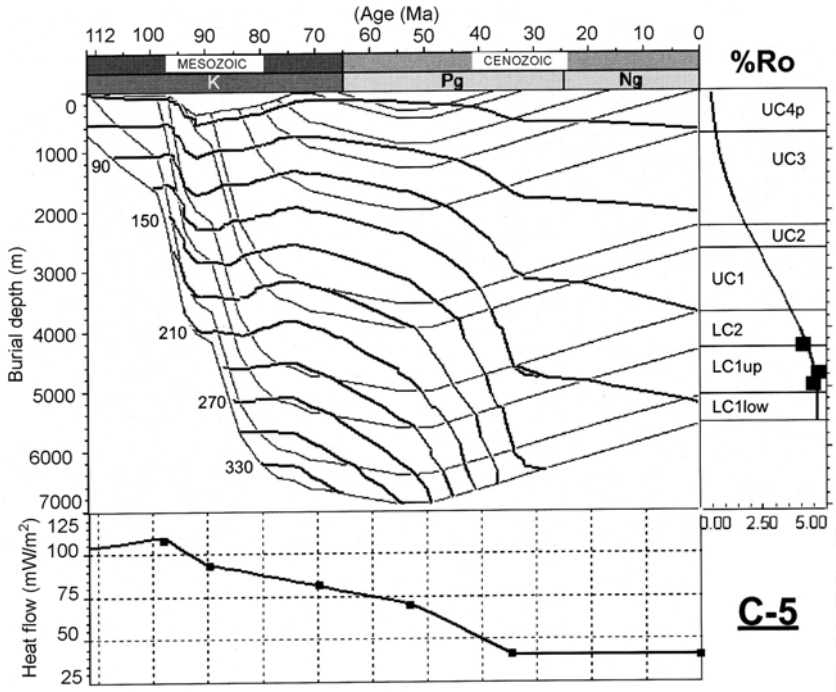

FIG. 6. (*above and facing page*) Proposed models for the wells Castillo-5, Treviño-3 and Lagran-1, showing burial and temperature history, heat-flow history, and calculated vitrinite reflectance curve, including calibration data (right).

and southern sectors. Meanwhile, in the central sector, a strongly subsiding trough was individualized (Miranda-Treviño syncline) as a consequence of the southward thrusting of the whole series. Throughout the Oligocene-Miocene (35–4.4 Ma), molassic materials were deposited in the trough and their distribution was controlled by palaeogeographic heights of diapiric origin.

In order to reconstruct the burial history of each well, definition of the different events (depositional, non-depositional and erosional) is required. We have considered deposit events as equivalent to the lithostratigraphic intervals from each well (Figs 4, 5). The thickness of each event has been corrected for dip (5–20º) and the presence of inverse faults (Treviño-3). The lithology of each event has been defined as a percentage mixture of shale, limestone and sandstone, bearing in mind petrographic observations and whole-rock mineralogy established by XRD. The age (Ma) assigned to each event corresponds to those established by Remane (2000) of the IUGS for the previous datings made by several authors (Ramírez del Pozo, 1971; IGME, 1987) in the study area.

Perhaps the most important variable to be considered in the reconstruction of the burial history of a sedimentary series is the estimation of eroded material thickness. In this study, eroded thickness in each well has been estimated on the basis of the available geological cartography (IGME, 1979; EVE, 1995), field observations, and lithological logs from the petroleum wells drilled in the region (Sangüesa, 1998). Although it may have been slightly diachronic, the onset of erosion has been situated in the Lower Lutecian (49 Ma) for the whole area, extending continuously in the northern (Castillo-5) and southern (Lagran-1) sectors, but interrupted in the central sector (Treviño-3) during the Oligocene–Miocene.

Thermal regime

Although the considerable volume of data from wells and geological sections in the Alava Block allows a precise reconstruction of its burial history, calibration data for the thermal history are rather scarce. Vitrinite reflectance data are only to be had for Lower Cretaceous materials from the three wells

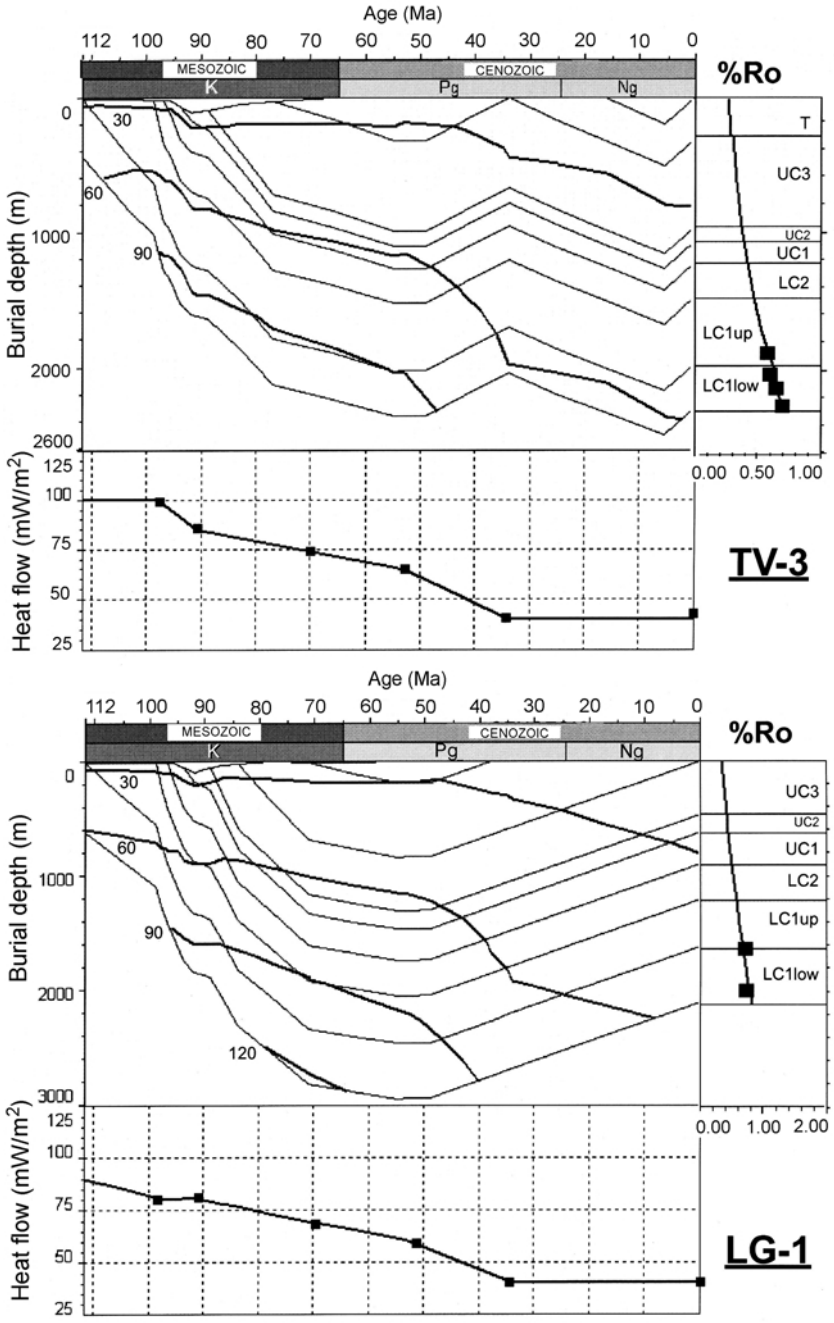

(Sangüesa *et al.*, 2000). Considering the wide range of geological history (100 Ma) for which calibration data is lacking, the thermal evolution model we propose is not the only possible solution, as it is possible to consider different thermal flow settings based on the available vitrinite data. Nevertheless, our knowledge about the geodynamic evolution of the basin allows us to constrain a thermal flow variation range for each stage of the evolution, taking into account the most common values for

basins in similar geodynamic settings (Allen & Allen, 1990).

The simplest evolution of the thermal flow in this basin would involve extending the present-day value (40 mW/m^2) to its whole geological history. Logically, the results from this supposition would not be in good agreement with the available calibration data from the wells due to the present-day hypothermic regime of the basin and the different geodynamic stages it has undergone during its evolution. As a starting point for determining a reasonable model for the thermal-flow evolution, we considered a number of fixed points (ages) in the basin history (Fig. 7), approximately marking the limits for the major stages of its geodynamic evolution (Olivet *et al.*, 1984; Boillot, 1988; Engeser & Schwentke, 1986; Rat, 1988; Vergés & García-Sáenz, 2001):

(1) Strike-slip basin from the Permian-Triassic to the middle Albian (110 Ma) due to the rotation and translation of the Iberian Subplate in relation to Eurasia, with involvement of the deep lithosphere.

(2) Extensional rift from the Albian (110 Ma) to the Campanian–Maastrichtian (71 Ma), with alkaline volcanism in the 110–85 Ma interval (Montigny *et al.*, 1986).

(3) Compressional basin (collisional) with subduction of the Iberain Subplate under the European Plate until the present day (71–0 Ma). During this stage, an orogenic paroxysm and a higher erosive ratio took place around the Eocene–Oligocene boundary (34 Ma).

The most common thermal-flow value based on the type of geodynamic setting has been assigned to the midpoint (Ma) of each of these stages and a progressive variation of those values has been interpolated between consecutive points. By means of successive iterations around these values, we have determined those showing the best agreement with available calibration data (Fig. 6). The result of this simulation shows a gradient in thermal flow, with a northward increase up to the Oligocene (34 Ma), which corresponds to the Alpine orogeny paroxysm (Fig. 7). From that time until the present day, models of the three wells show good agreement with current thermal flow (40 mW/m^2). The gradient in thermal flow may be related to the proximity of the Iberian Subplate boundary, the so-called North Pyrenean Fault, and its prolongation northwestwards in the Basque Cantabrian basin: the Leiza Fault (Martínez-Torres, 1991; Vergés & García-Senz, 2001;) and Kalamo Accident (Mathey *et al.*, 1999), located just north of our study area. Alkaline magmatic activity and HT-LP metamorphism, recorded in zones adjacent to the Alava Block, are related to these tectonic accidents.

DISCUSSION

Origin of clay minerals in the Alava Block

Clay mineral assemblages in the studied wells show important lateral and vertical variations if we compare Castillo-5 (northern domain) with the other

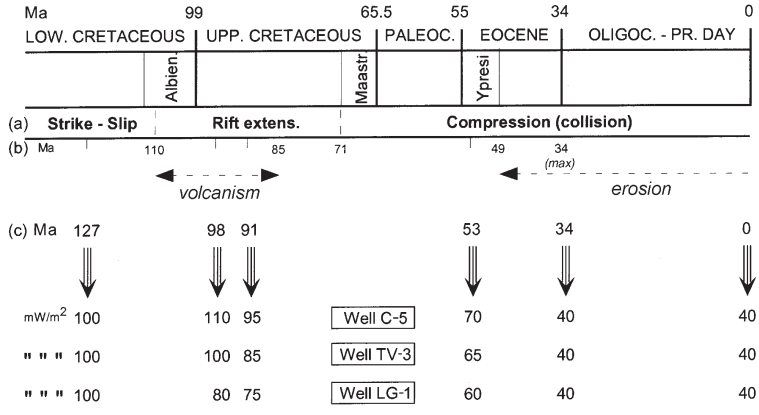

FIG. 7. Schematic bar for the geodynamic history of the Basque Cantabrian basin. The major tectonic events in the geodynamic history of basin (a), age (Ma) of the boundaries (b), and the midpoints (c) of the tectonic events, volcanism and maximum erosion are shown. Below the arrows: thermal flow values (mW/m^2) at the midpoints agree with calibration data in each well (see explanation in text).

two wells: Treviño-3 and Lagran-1 (central and southern domain, respectively). If we consider equivalent chronological periods, lateral variations in a sedimentary basin should be interpreted in the light of characteristics of sedimentary environments and paleogeographic position of the stratigraphic series considered. On the other hand, once the paleogeographic variable is known, vertical variations should be related to climatic factors and/or burial diagenesis, the latter acting as a modifying process of the initial mineralogical record.

In the upper part of the three wells, the mineral composition is qualitatively very similar, with mica and kaolinite contents increasing and smectite decreasing southward (Fig. 4). This distribution is the consequence of an increase in detrital character to the south, compatible with greater proximity to the source area.

The ubiquitous presence of smectite in Upper Cretaceous sediments is inherited from soils developed in the source area in the semi-arid climate that prevailed in this peri-Atlantic domain.

In the Lower Cretaceous of Lagran-1 and Treviño-3 (below LC2), smectite is absent, but I-S mixed-layer clays are also lacking (Fig. 4). This circumstance occurs in both wells in the same lithostratigraphic interval, at approximately the same burial depth (1835 and 1845 m, respectively), coinciding with a change from carbonates to detrital sediments. The general absence of smectite for most of the Lower Cretaceous in these two wells indicates that it was absent from the source area, probably as a consequence of the dominant subtropical climate (Sellwood & Price, 1994), suitable for kaolinite formation instead of smectite (Sangüesa *et al.*, 2000). During the Lower Cretaceous, physical erosion processes due to the rejuvenation of relief were important (Austrian phase of the Alpine orogeny); this accounts for the abundance of detrital mica (see below) in the sediments.

In Castillo-5, in a younger chronostratigraphic level (UC3), smectite was completely replaced by R1 and R3 type I-S interstratified minerals, more illite-rich with increasing depth. Here, in contrast to the other wells, where I-S mixed-layer clays are lacking, the absence of smectite must be related to diagenesis.

Kaolinite increases with depth throughout Lagran-1 and Treviño-3. This variation in kaolinite proportions may be explained by the greater distality from the source area for this sector of the basin during the Upper Cretaceous and by a change from warm and humid conditions in the Lower Cetaceous to a more seasonal arid climate in the Upper Cretaceous.

In contrast, in Castillo-5, kaolinite is absent below the carbonate-detrital lithological limit in the equivalent stratigraphic horizons. This absence cannot be explained by greater relative distality in this case, as equivalent sediments in more northern areas, i.e. more distal from the source area, do contain kaolinite (Arostegui *et al.*, 1993). Its disappearance must therefore be due to more advanced diagenesis as a consequence of the greater burial depth reached in this well. The greater permeability of these facies, sandy shales and sandstones, would have allowed the circulation of cation-rich (K, Mg, Fe) fluids, proceeding from the destruction of other minerals such as K-feldspar, ankerite, siderite and smectite. These cations, together with Al and Si from kaolinite dissolution, could have been the source for some of the illite and chlorite (Bartier *et al.*, 1998; Sangüesa *et al.*, 2000).

Chlorite is irregularly distributed throughout the wells. It is very scarce or even absent in Treviño-3 and Lagran-1. Nevertheless, in Castillo-5 chlorite is significant in the 1000–3600 m interval and is associated with different lithologies (Fig. 4); therefore, it cannot be related to the sedimentary environment or palaeogeographic position of this well. It seems to be closely related instead to the smectite-to-illite transformation as this chlorite is present when R0 is absent and shows a clear parallel with illite-rich (R1 and R3) mixed-layer clays. Chlorite could be a by-product originating from Fe, Mg and even Si from the smectite-to-illite transformation (Ahn & Peacor, 1985; Drief & Nieto, 2000; Masuda *et al.*, 2001).

Smectite-to-illite transformation in well Castillo-5

Well Castillo-5, in the northern part of the Alava Block, has the greatest burial rates in the region and is the only well showing smectite-to-illite evolution through the I-S, with increasing depth. In contrast to the other wells, smectite disappearance with depth takes place in an upper interval (UC3: Coniacian-Santonian) at a greater burial depth (2910 m; Table 2) and is not coincident with a lithostratigraphic change.

Bearing in mind that smectite was available in the source area from the end of the Lower

TABLE 2. Distribution of diagenetic zones and mineralogical events in wells from the Alava Block. C-5: Castillo-5, TV-3: Treviño-3 and LG-1: Lagran-1

	Present depth (m)	Burial depth (m)	Units (lower level)	*T* max. (ºC)
Well C-5				
R0	0–1640	1270–2910	UC4–UC3 (2/3 UC3)	160 (a)
R1>R3	1640–3700	2910–4970	UC3–2–1 (bottom UC1)	240
R3>R1	3700–4400	4970–5670	LC2 (bottom LC2)	270 (b)
I>I-S	4400–5583	5670–6853	LC1 (bottom well)	330
Kaolinite	0–3127	1270–4297	UC4–UC1 (2/3 UC1)	230 (c)
Well TV-3				
R0	0–1315	520–1835	T–LC2 (1/2 LC2)	70 (a)
Kaolinite	0–3000	520–3520	T–LC1 (bottom well)	100
Well LG-1				
R0	0–1010	835–1845	T–LC2 (1/2 LC2)	85 (a)
Kaolinite	0–2100	835–2935	T–LC1 (bottom well)	115

(a) Refers to the temperature for disappearance of smectite, (b) of R1 and (c) of kaolinite.

Cretaceous (LC2), the absence of smectite until the Coniacian-Santonian (lower third of interval UC3) in Castillo-5 must be a consequence of post-depositional changes, related to burial diagenesis. In this well, four zones, showing specific I-S interstratified clay assemblages (Fig. 4), have been differentiated from top to the bottom: (1) R0 (smectite-rich) zone, defined by the presence of smectite-rich mixed-layer I-S; (2) R1 zone, with illite-rich I-S interstratified clays (R1/R3 > 1); (3) R3 zone, with illite-rich I-S interstratified clays (R1/R3 < 1) and poorly crystallized illite (PCI); and (4) I (illite) zone, where mixed-layer I-S is very scarce.

The shallowest samples seem to evolve continuously, with the amount of illite layers in R0-type mixed-layer I-S increasing with depth, as shown by Arostegui *et al.* (1991). In deeper zones, different I-S types and illite coexist in each sample, showing a relative increase with depth in the proportions of the more illitic phase, but without apparent differences in quantitative parameters such as %I and CSDS of R1 and R3 phases (Table 1). These I-S interstratified clays finally disappear with depth below interval LC2, coinciding with the shale-sandstone limit; below this boundary, only illite is observed. Here, the origin of illite (PCI and WCI) cannot be explained in the general evolution scheme as smectite transformation of the original reactant, due to its absence in the equivalent sediments of the other two wells.

Smectite-to-illite evolution with progressive diagenesis can be assigned to two basic schemes, according to the literature: (1) continuous transformation of smectite layers to illite as burial diagenesis progresses, with intermediate illite-rich mixed-layer phases and the larger order in the more diagenetically evolved samples (Hower *et al.*, 1976; Drits *et al.*, 1997; Bauluz *et al.*, 2000); (2) discontinuous step-by-step transformation, with variations only in the proportion of coexisting phases, the composition of which basically remains constant (Dong & Peacor, 1996; Nieto *et al.*, 1996; Dong *et al.*, 1997).

The combined presence of R1 and R3 with practically constant characteristics along well Castillo-5, but varying relative proportions in the deepest samples, seem to point to a step-by-step illitization process.

The interpretation of XRD profiles in this study is consistent with transmission electron microscopy observations made by Nieto *et al.* (1996) of a composite stratigraphic sequence, to the north of the area, which covered the classic R0-R1-R3-illite range. The presence of illite as a discrete phase is generalized in all the samples (Fig. 5). Poorly crystallized illite (PCI) appears only in the deepest samples and well crystallized illite (WCI) is present in all the samples. In shales, the first appearance of PCI coincides with a clear decrease in the amount of R1; therefore, it represents a more advanced stage in illitization, which seems to advance towards an illitic end-member, with no smectite layers.

The presence of WCI showing similar characteristics (~100%I and 22–39 CSDS) is constant in all the samples along the entire C-5 well. It could correspond to diagenetic and/or detrital origins. The association of WCI with R0 in less diagenetically evolved samples indicates a detrital origin, at least partly.

Thermal modelling and clay mineralogy

The use of clay mineral changes during diagenesis as geothermometers has attracted attention for many years (see Eslinger & Glansmann, 1993). Smectite illitization (Hoffman & Hower, 1979); the disappearance of kaolinite (Boles & Franks, 1979; Frey, 1987; Giorgetti *et al.*, 2000), and the formation of chlorite (Barker & Pawlewicz, 1986; Hillier, 1993) are the processes most often referred to. One drawback to using these reactions as geothermometers is the need for both reactant phases and products to be in chemical equilibrium, a circumstance not common in diagenesis (Essene & Peacor, 1995, 1997). Most of the phases involved in such processes are metastable and, in addition to temperature, kinetic factors such as time, composition of initial phases and solutions, and permeability are key (Scotchman, 1987; Freed & Peacor, 1989; Huang *et al.*, 1993, Uysal *et al.*, 2000a; Abid *et al.*, 2004). Nevertheless, clay minerals evolve during diagenesis towards lower free-energy states; therefore, they are indicative of the reaction progress (Essene & Peacor, 1995). As a consequence, comparisons between the diagenetic grades of different basins based on temperature can only be made if the other variables are equivalent; likewise, the temperature variation of these transformations can be related to other kinetic factors. In the wells from the Alava Block, the sedimentary materials derived from a common source area and they can be grouped in chronostratigraphic units that have a similar lithology and are laterally correlated (Fig. 3). Therefore, the different stages observed in clay mineral evolution can be related to different temperatures.

These transformations have been defined by means of a number of mineralogical events, which have been located in the mean depth where the presence/absence or dominant character of specific phases have been observed. Each event we have defined in this way corresponds to a chronostratigraphic level in each well. Maximum burial depth and temperatures have been defined for the levels based on the burial and thermal history (Fig. 8). Table 2 shows that the present-day depth and temperature for each reference level are very different from those in the past as a consequence of the complex geological history of the Alava Block (see Thermal Modelling).

Smectite illitization may be monitored by means of the aforementioned prograde zones: R0–R1–R3–I. The lower limit of each corresponds to different chronostratigraphic levels, depth and temperature values in the wells. The temperature value for the onset of illitization in Castillo-5 is <90ºC, calculated for the least deeply buried sample (Fig. 5). In this well, the disappearance of smectite (R0), which marks the transition between zones R0 and R1, took place at a maximum temperature of 160ºC (Fig. 8), much higher than the values of 75–120ºC reported in the literature (Hoffman & Hower, 1979; Środoń & Eberl, 1984; Schegg & Leu, 1996; Uysal *et al.*, 2000b; Abid *et al.*, 2004).

In Lagran-1 and Treviño-3, the disappearance of smectite corresponds with temperature values of 85 and 70ºC, respectively (Fig. 8), and no sign of previous illitization has been observed in XRD profile decompositions (which are free of I-S peaks).

The temperature for the beginning of illitization in Castillo-5 is slightly greater than the maximum temperature reached by the stratigraphic levels that contain smectite in Treviño-3 and Lagran-1. Therefore, in these wells, the disappearance of smectite with depth is not as a result of the

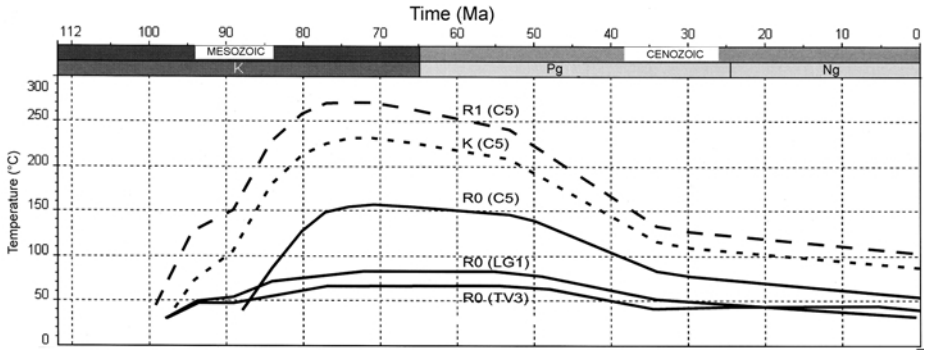

FIG. 8. Thermal history for those chronostratigrafic levels of each well where the disappearance of a clay mineral with depth has been observed. The disappearance of smectite (R0) (continuous line), R1-type I-S mixed layers (point line), and kaolinite (dotted line) are shown.

diagenetic temperature, but of the lack of smectite in the source area.

The transition between zones R1−R3, which can only be observed in Castillo-5 (UC-1 bottom), corresponds to 240ºC (Fig. 6) and the complete disappearance of R1 I-S around 270ºC (Fig. 8). These temperatures are also greater than those described in the literature (Abid *et al.*, 2004). Such high values may be related to the type of rocks (marls and marly limestones) in which the illitization took place. Retardation, and even reversals, of the general smectite illitization trend have frequently been described for this type of lithology. Low K contents in the sediment and the lack of necessary porosity preclude illite formation. Roberson & Lahan (1981) also suggested that Mg^{2+} and Ca^{2+} could inhibit illitization. The Alava Block, where the R1−R3 transition coincides in depth with the onset of shales and sandstones, is a significant example of such lithological control.

In the wells studied, diagenetic chlorite is restricted to Castillo-5. The temperature interval for chlorite formation in the Alava Block is 160−270ºC, coinciding with the development of I-S.

Kaolinite diagenetic instability is only observed in Castillo-5, in the UC1 interval, corresponding to a maximum temperature of 230ºC (Fig. 8). The stability of kaolinite is controlled by pH, ionic activity and temperature. Illite and/or chlorite can form at relatively low pH depending on K^+ or Mg^{2+} and Fe^{2+} availability. Kaolinite in diagenetic shales persists at maximum temperatures of ~200−210ºC (e.g. Boles & Franks, 1979; Giorgetti *et al.*, 2000). As for smectite illitization, retardation of this process in Castillo-5 would have been a consequence of the poor reactivity of marly lithologies, due to the low availability of K^+, Mg^{2+} and Fe^{2+}.

In the other wells, kaolinite is stable at depth, as maximum temperatures, 100 and 115ºC, respectively, were clearly insufficient for kaolinite transformation in spite of the sandy and shaley lithologies, where the high water/rock ratio would have favoured cation availability.

CONCLUSIONS

The original clay distribution was the result of detrital supply from the source area, mainly influenced by climate and intensity of erosion.

Only in the well Castillo-5 (north) can the influence of diagenesis be seen, due to deeper burial and a higher thermal regime throughout its geological history.

Illitization of smectite and the disappearance of kaolinite are the most characteristic mineralogical events, the results of diagenetic alteration.

Four zones of illitization have been differentiated: R0 with discrete smectite, R1 without smectite and with prevailing R1-type I-S mixed layers, R3 with mainly R3-type I-S mixed layers, and the I zone, with only illite.

Vitrinite-calibrated thermal models show that the present-day thermal flow of ~40 mW/m^2 is less than that of 60−100 mW/m^2 deduced for the past. This discrepancy is due to the different geodynamic stages the basin has undergone during its evolution. A northward-increasing thermal flow throughout the Cretaceous has also been deduced.

Thermal models allow temperatures of ~160ºC to be assigned for smectite disappearance, 240ºC for the R1/R3 transition, and 270ºC for R3/I. Kaolinite

is absent at 230ºC. In the wells Lagran-1 and Treviño-3, the absence of smectite with depth is due to its absence in the detrital supply, while kaolinite persists at depth throughout.

Calculated temperatures are greater than those described in the literature, due to an unfavourable lithological context for smectite illitization, constituted by marls and marly limestones (R0/R1) and shales (R1/R3). The scarcity of K-bearing phases and the low permeability of the medium explain the observed delay.

The scarcity of reactants and pathways implies that illitization could have taken place in a closed system, actually on the scale of the original smectite grains. In that case, illitization would have taken place with transport of cations by diffusion on a very local scale.

An increase in the relative proportion of the more illitic phases with depth has been observed with the CSDS of each phase. This means that the possibility of an Ostwald ripening mechanism for smectite illitization must be discounted. In such a low-porosity medium, the outer surfaces of crystallites of I-S and illite are limits for the growth of the layers, and illitization could only take place on a local scale.

ACKNOWLEDGMENTS

This work was supported by the project BTE2003-07867-C02-01 (DGI, Spanish Ministry of Science and Technology). The paper benefited from critical comments by S. Morad and an anonymous referee. We would like to thank Christine Laurin for revising the English.

REFERENCES

Abid I.A., Hesse R. & Harper J.D. (2004) Variations in mixed-layer illite/smectite diagenesis in the rift and post-rift sediments of the Jeanne d'Arc Basin, Grand Banks, offshore Newfoundland, Canada. *Canadian Journal of Earth Sciences*, **41**, 401–429.

Ahn J.H. & Peacor D.R. (1985) Transmission electron microscopic study of diagenetic chlorite in Gulf Coast argillaceous sediments. *Clays and Clay Minerals*, **33**, 165–179.

Allen P.A. & Allen J.R. (1990) *Basin Analysis: Principles and Applications.* Blackwell Scientific Publications, Oxford, UK, pp. 282–302.

Amiot M. (1982) El Cretácico superior de la Región Navarro-Cántabra. Pp. 88–111 in: *El Cretácico de España* (Departamento de Estratigrafía de la Facultad de Ciencias de la Universidad Complutense de Madrid & Instituto de Geología Económica del C.S.I.C., editors). Universidad Complutense, Madrid.

Amiot M., Floquet M. & Mathey B. (1983) Relations entre les trois domaines de sédimentation du Crétacé supérieur. In: Vue sur le Crétacé basco-cantabrique et nord-ibérique: Une marge et son arrière-pays, ses environnements sédimentaires. *Mémoires Géologiques de l 'Université de Dijon*, **9**, 169–176.

Arostegui J., Uriarte J.A. & Peña J.L. (1991) Smectite/illite distribution and temperature-time in Upper Cretaceous of the Alava Trough. Basque-Cantabrian basin (Spain). Pp. 47–52 in: *Proceedings of 7th Euroclay Conference* (M. Störr K.-H. Henning & P. Adolphi, editors). Ernst-Moritz-Arndt Universität, Greisfswald, Dresden, Germany.

Arostegui J., Nieto F., Ortega-Huertas M., Velasco F. & Zuluaga M.C. (1993) Mineralogía de arcillas y grado de diagénesis del Cretácico Inferior, en el flanco Sur del Anticlinorio de Bilbao. *Estudios Geológicos*, **49**, 55–70.

Barker C.E. & Pawlewicz M.J. (1986) The correlation of vitrinite reflectance with maximun temperature in humic organic matter. Pp. 79–83 in: *Paleogeothermics* (G. Buntebarth & L. Stegena, editors). Springer-Verlag, New York.

Bartier D., Buatier M., Lopez M., Potdevin J.L., Chamley H. & Arostegui J. (1998) Lithological control on the occurrence of chlorite in the diagenetic Wealden complex of the Bilbao anticlinorium (Basque-Cantabrian Basin, Northern Spain). *Clay Minerals*, **33**, 317–332.

Bauluz B., Peacor D.R. & Gonzalez Lopez J.M. (2000) Transmission electron microscopy study of illitization in pelites from the Iberian Range, Spain: Layer-by-layer replacement? *Clays and Clay Minerals*, **48**, 374–384.

Boillot G. & Malod J. (1988) The north and northwest Spanish continental margin: a review. *Revista de la Sociedad Geológica de España*, **1**, 295–316.

Boles J.R. & Franks S.G. (1979) Clay diagenesis in Wilcox sandstones of southwest Texas: implications of smectite diagenesis on sandstone cementation. *Journal of Sedimentary Petrology*, **49**, 55–70.

Dong H. & Peacor D.R. (1996) TEM observations of coherent stacking relations in smectite, I/S and illite of shales: evidence for MacEwan crystallites and dominance of $2M_1$ polytypism. *Clays and Clay Minerals*, **44**, 257–275.

Dong H., Peacor D.R. & Freed R.L. (1997) Phase relation among smectite, R1 illite-smectite, and illite. *American Mineralogist*, **82**, 379–391.

Drits V., Środoń J. & Eberl D.D. (1997) XRD measurement of mean crystallite thickness of illite and illite/smectite: Reappraisal of the Kubler index and the Scherrer equation. *Clays and Clay Minerals*,

45, 461–475.

Drief A. & Nieto F. (2000) Chemical composition of smectites formed in clastic sediments. Implications for the smectite-illite transformation. *Clay Minerals*, **35**, 665–678.

Engeser T. & Schwentke W. (1986) Towards a new concept of the tectogenesis of the Pyrenees. *Tectonophysics*, **129**, 233–242.

Eslinger E. & Glansmann J.R. (1993) Geothermometry and geochronology using clay minerals – an introduction. *Clays and Clay Minerals*, **41**, 117–118.

Essene E.J. & Peacor D.R. (1995) Clay mineral thermometry – A critical perspective. *Clays and Clay Minerals*, **43**, 540–553.

Essene E.J. & Peacor D.R. (1997) Illite and smectite: metastable, stable, or unstable? Further discussion and a correction. *Clays and Clay Minerals*, **45**, 116–122.

EVE (1995) *Mapa Geológico del País Vasco a escala 1/25.000*. Edited by Ente Vasco de la Energía (EVE), Bilbao, Spain.

Freed R.L. & Peacor D.R. (1989) Variability in temperature of the smectite/illite reaction in Gulf Coast sediments. *Clay Minerals*, **24**, 171–180.

Frey M. (1987) The reaction isograd kaolinite + quartz = pyrophyllite + H_2O, Helvetic Alps, Switzerland. *Schweizerische Mineralogische und Petrtographische Mitteilungen*, **67**, 1–11

García-Mondejar J. (1982) Aptiense y Albiense. Pp. 63–84 in: *El Cretácico de España* (Departamento de Estratigrafía de la Facultad de Ciencias de la Universidad Complutense de Madrid & Instituto de Geología Económica del C.S.I.C., editors). Universidad Complutense, Madrid.

Gier S. (2000) Clay mineral and organic diagenesis of the Lower Oligocene Schöneck Fishshale, western Austrian Molasse Basin. *Clay Minerals*, **35**, 709–717.

Giorgetti G., Mata M.P. & Peacor D.R. (2000) TEM study of the mechanism of transformation of detrital kaolinite and muscovite to illite/smectite in sediments of the Salton Sea Geothermal Field. *European Journal of Mineralogy*, **12**, 923–934.

Glansman J.R., Larter S., Briedis N.A. & Lundegart P.D. (1989) Shale diagenesis in the Bergen High area, North Sea. *Clays and Clay Minerals*, **37**, 97–112.

Gräfe K.U. & Wiedmann J. (1993) Sequence stratigraphy in the Upper Cretaceous of the Basco-Cantabrian Basin (northern Spain). *Geologische Rundschau*, **82**, 327–361.

Hillier S. (1993) Origin, diagenesis, and mineralogy of chlorite minerals in Devonian lacustrine mudrocks, Orcadian Basin, Scotland. *Clays and Clay Minerals*, **41**, 240–259.

Hoffman J. & Hower J. (1979) Clay mineral assemblages as low grade metamorphic geothermometers: Application to the thrust faulted disturbed belt of Montana. Pp. 55–79 in: *Aspects of Diagenesis* (P.A. Scholle & P.S. Schluger, editors). Special Publications, **26**, Society of Economic Paleontologists and Mineralogists, Tulsa, Oklahoma, USA.

Hower J., Eslinger E., Hower M.E. & Perry E.A. (1976) Mechanism of burial metamorphism of argillaceous sediment: 1. Mineralogical and chemical evidence. *Geological Society of America Bulletin*, **87**, 725–737.

Huang W.-L. Longo J.M. & Peaver D.R. (1993) An experimentally derived kinetic model for the smectite-to-illite conversion and its use as a geothermometer. *Clays and Clay Minerals*, **41**, 162–177.

IGME (1979) *Mapa geológico Nacional MAGNA a escala 1:50.000. Hojas de Haro, Miranda de Ebro, La Puebla de Arganzón, Orduña, Vitoria and Eulate*. Edited by Instituto Geológico y Minero de España, Madrid, Spain.

IGME (1987) *Contribución de la exploración petrolífera al conocimiento de la geología de España*. Edited by Instituto Geológico y Minero de España, Madrid, Spain, 465 pp.

Lanson B. (1997) Decomposition of experimental X-ray diffraction patterns (profile fitting): A convenient way to study clay minerals. *Clays and Clay Minerals*, **45**, 132–146.

Lanson B. & Besson G. (1992) Characterization of the end of smectite-to-illite transformation: Decomposition of X-ray patterns. *Clays and Clay Minerals*, **40**, 40–52.

Lanson B. & Velde B. (1992) Decompositión of X-ray diffraction patterns: A convenient way to describe complex diagenetic smectite-to-illite evolution. *Clays and Clay Minerals*, **40**, 629–643.

Martinez-Torres L.M. (1991) *El Manto de los Mármoles (Pirineo Occidental): geología estructural y evolución geodinámica*. PhD thesis, Universidad País Vasco, Spain.

Masuda H., Peacor D.R. & Dong H. (2001) Transmission electron microscopy study of the conversion of smectite to illite in mudstones of the Nankai Trough: contrast with coeval bentonites. *Clays and Clay Minerals*, **49**, 109–118.

Mathey B., Floquet M. & Martínez-Torres L.M. (1999) The Leiza palaeo-fault: role and importance in the Upper Cretaceous sedimentation and palaeogeography of the Basque Pyrenees (Spain). *Comptes Rendues de l 'Académie des Sciences de Paris*, **328**, 393–399.

Merriman R.J. (2005) Clay minerals and sedimentary basin history. *European Journal of Mineralogy*, **17**, 7–20.

Montigny R., Azambre B., Rossy M. & Thoizat R. (1986) K-Ar study of Cretaceous magmatism and metamorphism in the Pyrenees: age and length of

rotation of the Iberian peninsula. *Tectonophysics*, **129**, 257–273.

Moore D.M. & Reynolds R.C., Jr. (1997) *X-ray diffraction and the Identification and Analysis of Clay Minerals*, 2nd edition. Oxford University Press, New York, pp. 227–296.

Nieto F., Ortega-Huertas M., Peacor D.R. & Arostegui J. (1996) Evolution of illite/smectite from early diagenesis through incipient metamorphism in sediments of the Basque-Cantabrian Basin. *Clays and Clay Minerals*, **44**, 304–323.

Olivet J.L., Bonnin J., Beuzard P. & Auzende J.M. (1984) Cinematique de l'Atlantique nord et central. *Rapports Scientifiques et Techniques du Centre National pour l 'Exploitation des Oceans*, **54**, 108 pp. Paris, France.

Pearson M.J. & Small J.S. (1988) Illite-smectite diagenesis and paleotemperatures in northern North Sea Quaternary to Mesozoic shale sequences. *Clay Minerals*, **23**, 109–132.

Ramírez del Pozo J. (1971) Bioestratigrafía y microfacies del Jurásico y Cretácico del Norte de España (Región Cantábrica). *Memorias del Instituto Geológico y Minero de España*, **78**, 357 pp.

Rat P. (1988) The Basque-Cantabrian basin between the Iberian and European plates: Some facts but still many problems. *Revista de la Sociedad Geológica de España*, **1**, 327–348.

Remane J. (2000) *International Stratigraphic Chart, with Explanatory Note*. Sponsored by ICS, IUGS and UNESCO, 31st International Geological Congress, Rio de Janeiro, 16 pp.

Roberson H.E. & Lahan R.W. (1981) Smectite to illite conversion rates: effects of solution chemistry. *Clays and Clay Minerals*, **29**, 129–135.

Sangüesa F.J. (1998) *La diagenesis en el Bloque Alavés de la Cuenca Vasco-Cantábrica. Distribución, modelización y aplicaciones*. PhD thesis, Universidad de País Vasco, Spain.

Sangüesa F.J., Arostegui J. & Suárez-Ruiz I. (2000) Distribution and origin of clay minerals in the Lower Cretaceous of the Alava Block (Basque-Cantabrian basin. Spain). *Clay Minerals*, **35**, 393–410.

Schegg R. & Leu W. (1996) Clay mineral diagenesis and thermal history of the Thonex Well, Western Swiss Molasse Basin. *Clays and Clay Minerals*, **44**, 693–705.

Scotchman I.C. (1987) Clay diagenesis in Kimmeridge Clay Formation, onshore UK, and its relation to organic maturation. *Mineralogical Magazine*, **51**, 535–551.

Sellwood B.W. & Price G.D. (1994) Sedimentary facies as indicators of Mesozoic paleoclimate. Pp. 17–25 in: *Paleoclimates and their Modelling – with special reference to the Mesozoic era* (J.R.L. Allen, B.J. Hoskins, B.W. Sellwood, R.A. Spicer & P.J. Valdes, editors). Chapman & Hall/Royal Society, UK.

Środoń J. & Eberl D.D. (1984) Illite. Pp. 495–544 in: *Micas* (S.W. Bailey, editor). Reviews in Mineralogy, **13**. Mineralogical Society of America, Washington D.C., USA.

Tissot B.P., Pelet R. & Ungerer Ph. (1987) Thermal history of sedimentary basins, maturation indices and kinetics of oil and gas generation. American Association of Petroleum Geologists Bulletin, **71**, 1445–1466.

Uysal I.T., Golding S.D. & Audsley F. (2000a) Clay-mineral authigenesis in the Late Permian coal measures, Bowen Basin, Queensland, Australia. *Clays and Clay Minerals*, **48**, 351–365.

Uysal I.T., Glikson M., Golding S.D. & Audsley F. (2000b) The thermal history of the Bowen Basin, Queensland, Australia: vitrinite reflectance and the clay mineralogy of Late Permian coal measures. *Tectonophysics*, **323**, 105–129.

Velde B. & Lanson B. (1993) Comparison of I-S transformtion and maturity of organic matter at elevated temperatures. *Clays and Clay Minerals*, **41**, 178–183.

Vergés J. & García-Saenz J. (2001) Mesozoic evolution and Cainozoic inversion of the Pyrenean Rift. Pp. 187–212 in: Peri-Tethyan Rift/Wrench Basins and Passive Margins (P.A. Ziegler, W. Cavazza, A.H.F. Robertson & S. Crasquin-Soleau, editors). *Mémoires du Muséum National d'Histoire Naturelle*, **186**, Paris, France.

Waples D.W., Kamata H. & Suizu M. (1992) The art of maturity modeling; Part 1, Finding a satisfactory geologic model. *American Association of Petroleum Geologists Bulletin*, **76**, 31–46.

Yahi N. Schaefer R.G. & Littke R. (2001) Petroleum generation and accumulation in the Berkine Basin, Eastern Algeria. *American Association of Petroleum Geologists Bulletin*, **85**, 1439–1467.